Laboratory investigations of the interaction between benzene and bare silicate grain surfaces

J. D. Thrower,[1]⋆ M. P. Collings,[1] F. J. M. Rutten[2] and M. R. S. McCoustra[1]

[1]*School of Engineering and Physical Sciences, Heriot-Watt University, Edinburgh EH14 4AS*
[2]*School of Pharmacy and iEPSAM, Keele University, Keele ST5 5BG*

ABSTRACT

Experimental results on the thermal desorption of benzene (C_6H_6) from amorphous silica (SiO_2) are presented. The amorphous SiO_2 substrate was imaged using atomic force microscopy, revealing a surface morphology reminiscent of that of interplanetary dust particles (IDPs). Temperature-programmed desorption (TPD) experiments were conducted for a wide range of C_6H_6 exposures, yielding information on both C_6H_6–SiO_2 interactions and the C_6H_6–C_6H_6 interactions present in the bulk C_6H_6 ice. The low-coverage experiments reveal complicated desorption behaviour that results from both porosity and roughness in the SiO_2 substrate, and repulsive interactions between C_6H_6 molecules. Kinetic parameters were obtained through a combination of direct analysis of the TPD traces and kinetic modelling, demonstrating the coverage dependence of both desorption energy and pre-exponential factor. Experiments were also performed whereby the pores were blocked by pre-exposure of the SiO_2 to water vapour. C_6H_6 was observed to be adsorbed preferentially on the SiO_2 film not covered by H_2O at the temperature at which these experiments were performed. This observation means that intermolecular repulsion likely becomes important at smaller C_6H_6 exposures on grains with a H_2O mantle. Kinetic modelling of C_6H_6 multilayer desorption yields kinetic parameters in good agreement with previous studies, with the SiO_2 having little impact on the desorption beyond the first few layers.

Key words: molecular data – molecular processes – methods: laboratory – ISM: molecules.

1 INTRODUCTION

Carbon is thought to exist in many forms throughout the interstellar medium (ISM). In particular, polycyclic aromatic hydrocarbons (PAHs) are generally considered to be one of the most important classes of carbon-bearing molecule (Ehrenfreund & Sephton 2006). PAHs have been proposed as carriers of both the diffuse interstellar bands (DIBs) (Duley 2006 and references therein) and the unidentified infrared bands (UIRs) (Allamandola, Hudgins & Sandford 1999). Absorption features corresponding to the UIRs have been observed towards several protostellar objects and towards the Galactic Centre (Bregman & Temi 2001 and references therein). PAH emission features have been observed in a wide range of environments (see e.g. Kaneda, Onaka & Sakon 2005; Lagadec et al. 2006; Flagey et al. 2006; Kassis et al. 2006; Smith et al. 2007), demonstrating their ubiquitous nature. As with many gas-phase molecules, it is likely that PAHs are also present mixed in the water (H_2O) ice dominated mantles surrounding grains in the dense ISM under suitably cold conditions. Laboratory spectra of PAHs in appropriate ice matrices

are essential in aiding the interpretation of observational spectra. To this end, there have been several experimental studies of the infrared absorption spectra of PAH/H_2O ice mixtures (Sandford, Bernstein & Allamandola 2004; Bernstein, Sandford & Allamandola 2005; Bernstein et al. 2007).

We are currently undertaking work to investigate the irradiation of PAHs with both photons and electrons. As a first step for understanding the relevant processes, we are focusing on benzene (C_6H_6), primarily for reasons of experimental convenience, before considering simple PAH species and their heterocyclic analogues, including pyridine (C_5H_5N). As ultraviolet (UV) absorption characteristics of small PAHs and C_6H_6 are similar, any knowledge obtained from studies of this simpler system will contribute positively to our understanding of processes involving PAH larger species. Furthermore to aid in interpreting the results of irradiation experiments, it is necessary to understand the nature of the pre-irradiated ice. For example, in our recently reported experimental measurements of the photodesorption of C_6H_6 from H_2O ice (Thrower et al. 2008), the desorption of both C_6H_6 and H_2O was found to depend strongly on the morphology of the ices. It is clear that a more detailed understanding of the interactions between both C_6H_6 and H_2O and the underlying substrate is required. As far as we are aware, there

⋆E-mail: jdt5@hw.ac.uk

have been no experimental studies of the interaction between C$_6$H$_6$ and suitable grain mimics. We have chosen a grain mimic based on a thin film of amorphous silica in order to represent the silicate grain population. Compared to our previous study of the desorption of CO from meteorite nanoparticles (Mautner et al. 2006), such a substrate is likely to be more reproducible in the laboratory. The surface will also be chemically much less complex, allowing a more fundamental approach to the study of adsorption on the grain mimic surface to be adopted.

Evidence suggests that C$_6$H$_6$ is readily destroyed in diffuse regions by interaction with protons and UV photons (Ruiterkamp et al. 2005). However, in denser regions and circumstellar envelopes where molecules are more shielded from the interstellar radiation field, the C$_6$H$_6$ lifetime is expected to be much longer. Evidence for this has come from the *Infrared Space Observatory* mission with the observation of C$_6$H$_6$ in the carbon-rich protoplanetary nebula (PPN) CRL 618, accompanied by, C$_4$H$_2$ and C$_6$H$_2$ (Cernicharo et al. 2001). These observations have suggested that a significant amount of organic chemistry occurs in C-rich PPNe. Various mechanisms have been put forward for the synthesis of C$_6$H$_6$ in environments exhibiting different physical and chemical conditions. In the dense ISM, the formation of hydrocarbon species, including C$_6$H$_6$, via a gas-phase ion neutral scheme involving atomic hydrogen has been proposed (McEwan et al. 1999). A mechanism initiated by reaction of a range of ions with acetylene (C$_2$H$_2$) has been shown to account for the significantly higher C$_6$H$_6$ abundance observed in CRL 618 (Woods, Miller & Zijlstra 2002). A series of reactions based on soot formation involving C$_2$H$_2$ has also be proposed as a likely route for the synthesis of C$_6$H$_6$ and PAHs in circumstellar envelopes (Frenklach & Feigelson 1989; Cherchneff, Berker & Tielens 1992). It has been suggested that organometallic catalysis in these environments may lead to an increased C$_6$H$_6$, and therefore PAH, production rate (Ristorcelli & Klotz 1997). In protostellar discs, a different mechanism has been proposed (Woods & Willacy 2007), whereby C$_6$H$_6$ is formed via c-C$_6$H$_7^+$ (where c- denotes a cyclic species). Following adsorption of this protonated species on a grain surface, proton transfer and charge neutralization yield adsorbed C$_6$H$_6$ and H. The efficiency of this proton transfer mechanism on returning C$_6$H$_6$ to the gas phase will depend on how strongly the adsorbed C$_6$H$_6$ is bound to the grain surface. In this work, it was noted that values in the existing literature for the desorption energy of a C$_6$H$_6$ molecule from a bare grain surface can range from 4700 K to as much as 7500 K (Arnett, Hutchinson & Healy 1988; Hasegawa & Herbst 1993; Lozovik, Popov & Letokhov 1995; Garrod & Herbst 2006). In only one of these studies (Arnett et al. 1988) is a value derived experimentally, with gas–solid chromatography being used to obtain the desorption energy from graphite, yielding a value of 39 ± 3 kJ mol^{-1} (4750 ± 360 K). This is clearly not the most appropriate experiment on which to base an understanding of adsorption to interstellar grains.

There have been many experimental studies of the adsorption of C$_6$H$_6$ on both single crystal and polycrystalline metal surfaces (See e.g. Jakob & Menzel 1989; Haq & King 1996; Rockey, Yang & Dai 2006). On many substrates, C$_6$H$_6$ has been found to adsorb plane parallel to the substrate, bonding via the π electrons. Amorphous silica is widely used as a support for catalysts and has been studied extensively. It is well known that exposure of silica surfaces to H$_2$O results in reaction to form surface hydroxyl (OH) groups known as silanols. The resulting hydrophilic surface has been studied recently by *ab inito* methods (Tielens et al. 2008). H$_2$O was shown to interact with three binding sites with adsorption energies of 44, 46 and 50 kJ mol^{-1}, characteristic of hydrogen bonding interactions. C$_6$H$_6$

has been shown to form weak hydrogen bonds to water via the aromatic ring (Suzuki et al. 1992), indicating that such bonds may also be important in the adsorption of C$_6$H$_6$ on a hydroxylated SiO$_2$ surface.

2 EXPERIMENTAL METHODS

The experiments described here were conducted in a stainless steel ultrahigh vacuum (UHV) chamber that has been described in detail elsewhere (Oakes 1994). The chamber is pumped by a combination of liquid-nitrogen-trapped diffusion pumps and a titanium sublimation pump. Following bakeout to remove water adsorbed on internal surfaces, a base pressure of 2×10^{-10} torr is routinely obtainable. The substrate was a 10 mm diameter, polished stainless steel disc that was attached to molybdenum support posts on an oxygen-free high-conductivity copper mount by tantalum wires. Experiments were conducted on both the polished stainless steel surface and a thin film of SiO$_2$ deposited on this surface in order to gain some insight into the effect of the SiO$_2$ on adsorption. The SiO$_2$ films were deposited in a separate chamber by electron beam evaporation of bulk material. The substrate was maintained at room temperature during the evaporation, and ∼200 nm of SiO$_2$ were deposited as measured by a quartz crystal microbalance situated close to the substrate. The film thickness of 200 nm was chosen in order to provide a film thick enough that pathways to the stainless steel substrate are limited without introducing interference effects into any future infrared studies. The substrate was cleaned by heating to 500 K for 15 min before cooling, prior to conducting experiments.

The substrate was cooled to a base temperature of around 115 K by a liquid nitrogen reservoir in thermal contact with the sample mount. This temperature is significantly higher than that of dust grains in dense clouds (10–20 K), however, preliminary experiments on a system with a substrate base temperature of 10 K (not shown) have demonstrated that C$_6$H$_6$ does not desorb below 120 K. Similarly, previous experiments (Fraser et al. 2001; Bolina, Wolff & Brown 2005) have also shown that H$_2$O does not desorb below the base temperature used in the experiments described here. The substrate could be heated resistively by passing current through the support wires. A K-type (Chromel-Alumel) thermocouple, spotwelded to the edge of the substrate, was used for temperature monitoring. A programmable controller (Eurotherm) was used to provide a linear heating ramp (β) of 0.1 ± 0.02 K s^{-1} during temperature-programmed desorption (TPD) experiments.

UV-spectroscopy grade C$_6$H$_6$ (Fluka) and deionized H$_2$O were further purified by repeated freeze-pump-thaw cycles on a dedicated stainless steel preparation line pumped by a diffusion pump. To avoid cross-contamination, the C$_6$H$_6$ and H$_2$O were purified on independent manifolds, each with a fine leak valve for dosing into the main UHV chamber. Layers of C$_6$H$_6$ and H$_2$O were deposited on to the substrate by backfilling the chamber to a pressure as measured by an uncalibrated ion gauge. Exposures are reported in Langmuir (1 L = 1 × 10^{-6} torr s). Though it is not possible to accurately determine coverages with our experimental arrangement, the surface concentration of adsorbed molecules was estimated by using a simple collision theory, assuming a sticking probability of unity and an ion gauge sensitivity correction factor of 6 for C$_6$H$_6$ (Waddill & Kesmodel 1985).

The desorption of H$_2$O and C$_6$H$_6$ molecules during TPD experiments was monitored using a quadrupole mass spectrometer (QMS) (modified VG Micromass PC300D) with a cross-beam ion source and channel electron multiplier detector that was operated in analogue (current) mode. The QMS was housed in a

differentially pumped stainless steel chamber within the main UHV chamber. This arrangement reduces the background signal from residual gases within the main chamber. The QMS chamber incorporated a small tube in line with the ionization region. During TPD experiments, the substrate was moved close to the opening of this tube, which provided a line of sight to the ionization region. This significantly reduced the detection of molecules desorbing from other surfaces such as the mount and support wires. C_6H_6 and H_2O were detected by their parent ions with masses 78 and 18 m_u respectively. The thermocouple voltage was recorded simultaneously by the QMS software following pre-amplification, and subsequently converted to temperature using a previously obtained calibration curve.

3 RESULTS AND DISCUSSION

In order to assess the nature of the amorphous silica substrate used in these experiments, the surface morphology of the film was investigated using an atomic force microscopy (AFM) prior to mounting in the UHV chamber. AFM images were obtained with a silicon nitride tip operated in constant force contact mode. At present, there is no detailed understanding of the morphology of interstellar grains. A reasonable approximation can be made by considering that of interplanetary dust particles (IDPs). Whilst it is important to recognize that IDPs are likely to have been processed during the formation of the Solar system, we consider only the overall structure of the surface, neglecting any chemical modifications which are not represented in our grain mimic. Fig. 1 shows a $20 \times 20\ \mu m$ region of the amorphous silica surface along with a scanning electron

(a)

60 nm / 1 μm
1 μm

(b)

1 μm

Figure 1. (a) Constant force contact mode AFM image of the amorphous SiO_2 substrate used in these experiments compared with (b) an SEM image of an IDP. For clarity, the AFM image has been exaggerated in the vertical direction.

microscope (SEM) image of an IDP.[1] For clarity, the AFM image has been exaggerated in the vertical direction. The amorphous silica surface appears to reproduce the morphology of the IDP well on a similar length-scale. The likely presence of pores on grain surfaces, which are not present with the polycrystalline Au substrate used in our earlier studies, may have important consequences for the morphology of adsorbates.

Fig. 2 shows TPD traces for the desorption of C_6H_6 from the bare amorphous silica surface for low, intermediate and large exposures of C_6H_6. In all cases, the C_6H_6 was deposited whilst the substrate was at its base temperature of 115 K, and the TPD traces were obtained with a heating rate, β, of 0.1 K s^{-1} to a temperature of 210 K, above which no further C_6H_6 desorption was detected. At the smallest exposure, a single desorption feature (Peak A) is present at around 180–190 K. As the exposure is increased, this peak moves to lower temperature whilst retaining the same high-temperature tail. Peak A appears to saturate between 0.5 and 1 L with further exposure leading to the appearance of a much sharper peak (Peak B) centred around 140 K. This peak continues to shift to lower temperature, though to a lesser extent than that observed for Peak A. As will be discussed, we attribute Peak A to a combination of C_6H_6 desorption from the surface of the SiO_2 and from within pores in the film. Peak B can be attributed to desorption of C_6H_6 from a more crowded layer formed on the surface of the SiO_2 film when filling of the pores is complete. At around 3 L, Peak B saturates and Peak C begins to grow at around 140 K. This peak is attributed to desorption from the first few multilayers of the solid C_6H_6 ice. It is clear that the leading edges of this peak are not coincident as would be exhibited by zero-order desorption. This can be interpreted in terms of a fractional-order desorption process. This may arise either when islands of C_6H_6 form upon the first layer or as a consequence of the inherent roughness of the underlying SiO_2 film. It is also interesting to note that as this peak grows, Peak B is reduced indicating that desorption of the C_6H_6 monolayer cannot occur until multilayer desorption begins. Beyond around 10 L, a single desorption peak (Peak D) dominates the TPD traces with no monolayer peak being resolved. This peak displays coincident leading edges for all exposures up to the maximum investigated (500 L), and can be attributed to zero-order desorption from bulk C_6H_6 ice.

The desorption from the lowest exposures of C_6H_6 reflects the nature of the surface/adsorbate interaction. Typically, desorption from a submonolayer coverage on a flat, well-ordered surface will yield a narrow, slightly asymmetric peak, characteristic of first-order desorption kinetics. Here, the desorption shows a broad tail extending to high temperature which reflects the rather more complicated nature of the SiO_2 surface. This tail can be interpreted in two ways. If the surface, rather than having one type of binding site with a characteristic desorption energy, has a distribution of binding sites, a molecule will preferentially adsorb in the sites with higher binding energies. As the coverage is increased, binding sites with progressively lower binding energies will be occupied. Desorption will occur from those sites with the lowest binding energy first, with the desorption profile reflecting the distribution of binding energies. However, whilst a small distribution of binding energies on this surface might be expected, it is unlikely that this would lead to C_6H_6 desorption over such a broad range of temperatures. An alternative explanation is that the observed tail is due
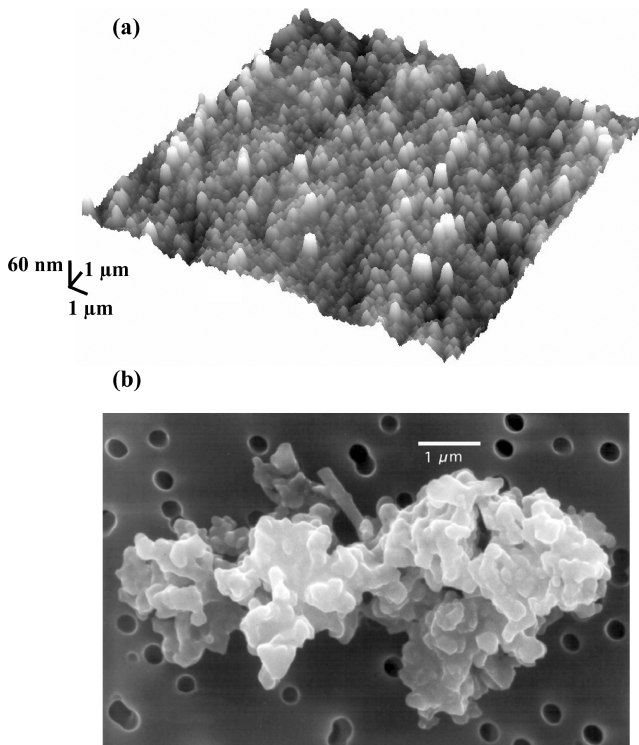
[1] IDP image obtained from Wikipedia with permission from E. K. Jessberger. Retrieved from http://en.wikipedia.org/wiki/Image:Porous_chondriteIDP.jpg on 2008 June 12.
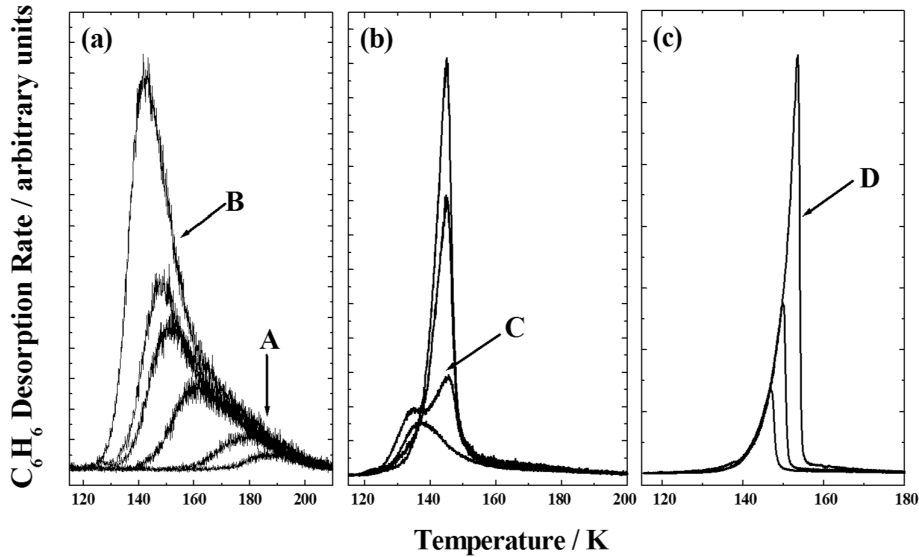
Figure 2. TPD traces for C$_6$H$_6$ desorption from amorphous SiO$_2$. C$_6$H$_6$ exposures displayed are (a) 0.1, 0.2, 0.5, 0.7, 0.8 and 1 L, (b) 2, 3, 4 and 5 L and (c) 10, 20 and 50 L.

to the presence of pores in the SiO$_2$. This behaviour, where the peak gradually shifts to lower temperature with increasing coverage, has previously been observed in the desorption of CO from a highly porous H$_2$O film deposited at 10 K (Collings et al. 2003). This was interpreted as being due to molecules bound within pores desorbing and then re-adsorbing elsewhere on the pore surface. It may then take several of these desorption, re-adsorption steps until the C$_6$H$_6$ desorbs from the SiO$_2$ substrate into the UHV chamber itself, resulting in a much broader desorption profile. In order to investigate this further, experiments were performed where the surface was first exposed to a small amount of H$_2$O. C$_6$H$_6$ was then deposited to an exposure of 0.5 L. Fig. 3 shows TPD traces for the desorption of 0.5 L of C$_6$H$_6$ from bare SiO$_2$ and SiO$_2$ that had been pre-exposed to small exposures of H$_2$O. If the broad tail of Peak A were due to a wide distribution of binding energies, then at low-coverages H$_2$O would be expected to bind preferentially at those sites with the highest binding energy. The C$_6$H$_6$ would then be adsorbed in sites with lower binding energies resulting in a narrowed desorption tail, i.e. the one that is reduced in intensity at higher desorption temperatures. However, in these experiments the tail is reduced at lower desorption temperatures with the development of a two peak profile. This indicates that Peak A is not due to a significant distribution of binding energies. As the amount of H$_2$O to which the SiO$_2$ surface is pre-exposed is increased, Peak A is reduced to progressively higher desorption temperatures. As Peak A is reduced, the C$_6$H$_6$ desorption comes to be dominated by a peak similar to Peak B in Fig. 2. These observations can be explained by considering the relative mobilities of C$_6$H$_6$ and H$_2$O. At the substrate temperature used in these experiments, C$_6$H$_6$ will be more mobile than H$_2$O upon adsorption, and will adsorb throughout the pore network when H$_2$O is not present. On the other hand, H$_2$O, upon adsorption, will be relatively immobile as a consequence of strong hydrogen bonding to SiO$_2$ surface OH groups, and will not penetrate as deeply into the pore network as C$_6$H$_6$. C$_6$H$_6$ dosed after small amounts of H$_2$O will therefore still be able to adsorb deep within the pores, with the desorption profile displaying the high-temperature tail. The stronger interaction between H$_2$O and the SiO$_2$ surface means that pre-deposited H$_2$O cannot be displaced by C$_6$H$_6$. The total number of sites available for C$_6$H$_6$ adsorption
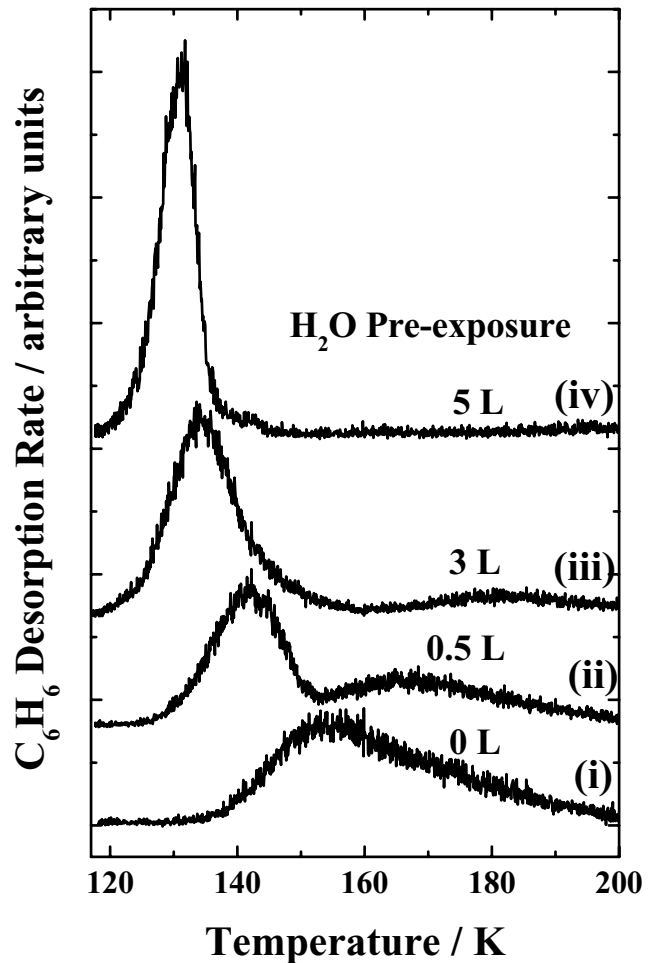

Figure 3. TPD traces resulting from the desorption of 0.5 L C$_6$H$_6$ from (i) bare amorphous SiO$_2$ and SiO$_2$ that had been exposed to, (ii) 0.5 L, (iii) 3 L and (iv) 5 L H$_2$O.

within the pore network will therefore be reduced, particularly near the surface, resulting in the observed reduction in the desorption profile from lower temperatures. Exposure to larger amounts of H_2O will block the pathways to the pore network resulting in C_6H_6 adsorbing preferentially on the parts of the SiO_2 film that remain exposed, rather than on the surface of the pre-adsorbed H_2O. This gives rise to the appearance, at higher water pre-exposures, of Peak B which was previously attributed to the desorption of C_6H_6 from the surface of the SiO_2 film. The non-wetting behaviour of C_6H_6 on H_2O has also been observed in experiments where C_6H_6 was adsorbed on a thick layer of H_2O sufficient to completely cover the SiO_2 surface (data not shown). Multilayer-like desorption was observed for all exposures, indicating the formation of isolated islands of C_6H_6 dominated by C_6H_6–C_6H_6 interactions on the H_2O ice surface. A detailed study of the interaction of C_6H_6 with H_2O ice surfaces will be the subject of a future publication. It is likely that during exposure of the SiO_2 film to C_6H_6, C_6H_6 adsorbs both within the pores *and* on the surface of the film, given that the range of binding energies is small. However, increased mobility during heating may cause surface-adsorbed C_6H_6 to migrate to within the pore network prior to desorption. Further evidence for the impact of surface roughness and the presence of pores comes from a comparison with initial TPD experiments performed with the polished stainless steel disc prior to the deposition of the SiO_2 film (data not shown). No high-temperature tail was observed in the TPD trace, and the monolayer peak was saturated at around 0.7 L. Comparing this to the observed monolayer saturation at around 3 L on amorphous SiO_2 gives an apparent surface area increase of between fourfold and fivefold. This results from both adsorption in pores and an increased surface roughness.

In order to obtain values for the kinetic parameters for the desorption processes, a combination of direct analysis of the experimental TPD traces and kinetic modelling was used. To describe the desorption kinetics, the rate of desorption can be written in terms of the surface concentration of the adsorbed species:

$$r_{des} = -dN/dt = k_{des}N^n, \qquad (1)$$

where N is the surface concentration of the adsorbed species in molecules cm^{-2}, n is the desorption order and k_{des} is the rate coefficient, which can be expressed as

$$k_{des} = \nu \exp(-E_{des}/k_B T), \qquad (2)$$

where ν is the pre-exponential factor, E_{des} is the desorption energy in Joules and T is the surface temperature in kelvin. The units of ν depend on the order, being molecules $cm^{-2}\ s^{-1}$ and s^{-1} for $n = 0$ and 1, respectively. If the temperature ramp is linear, as was the case in these TPD experiments, the rate equation can be expressed as (Attard & Barnes 1998)

$$dN/dT = (N^n \nu/\beta) \exp(-E_{des}/k_B T), \qquad (3)$$

where β is the heating rate in K s^{-1}. If the pumping speed is sufficiently high, as expected in our UHV system, the signal from the QMS is directly proportional to dN/dT.

It is clear that in order to obtain the kinetic parameters for a particular TPD trace, the surface concentration of adsorbed molecules is required. We are able to obtain approximate surface concentrations by the application of a simple collision theory (Atkins & de Paula 2002), in which the collision frequency, Z in molecules $m^{-2}\ s^{-1}$, for molecules striking a surface can be expressed as
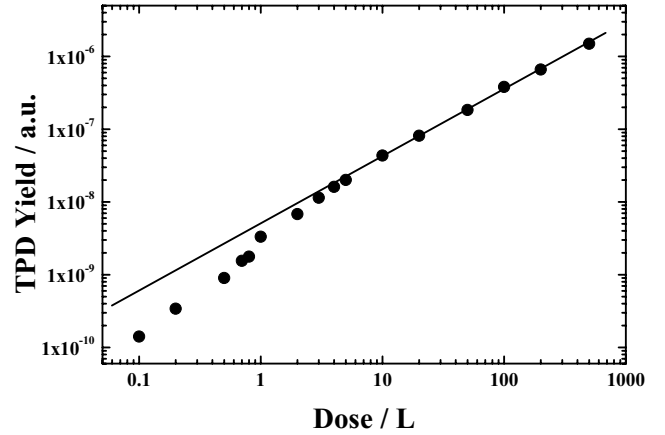
$$Z = P/(2\pi m k_B T)^{1/2}, \qquad (4)$$

Figure 4. The TPD yield (integrated peak area), which is proportional to the surface concentration of adsorbed C_6H_6, as a function of exposure in L. This reveals a significant overestimate of actual C_6H_6 exposure at low coverages as observed by deviation from linearity. Surface concentrations were therefore obtained by comparison of the TPD yield with that for 500 L.

where P is the partial pressure of the species being deposited, m is the molecular mass in kg and T is the gas temperature (i.e. 298 K). Multiplication by the dosing time yields the surface concentration assuming a sticking coefficient of unity. The pressure reading from the ion gauge must be scaled by the appropriate sensitivity factor, 6 in the case of benzene (Waddill & Kesmodel 1985). Small variations in the dosing conditions can impact on the resulting surface concentration. For this reason, the highest dose of 500 L was taken to be exactly 500 L. The TPD trace for 500 L was integrated to obtain the TPD yield. Actual values were then obtained for the other doses by comparison of TPD yield with that obtained for 500 L. Fig. 4 shows how the TPD yield varies with increasing dose. It is clear that there are significant variations at the lowest dose, with actual doses being significantly smaller than expected. Comparison with the highest dose, expected to be the most accurate, is therefore required.

Kinetic modelling was performed using the Chemical Kinetics Simulator (CKS) package[2] (Houle & Hinsberg 1995) to stochastically integrate the differential equations describing the desorption process. We have used this approach previously in the analysis of the desorption of pure water ice (Fraser et al. 2001) and of CO from a water ice matrix (Collings et al. 2003). A simple mechanism for the desorption process was constructed:

$$C_6H_6\ (ads) \rightarrow C_6H_6\ (g), \qquad (5)$$

$$C_6H_6\ (g) \rightarrow C_6H_6\ (pumped), \qquad (6)$$

where the concentration of C_6H_6 (ads) is equivalent to N, the surface concentration of adsorbed molecules. Equation (5) describes the desorption step and equation (6) describes the removal of benzene from the UHV chamber by the pumping system, which is proportional to the concentration of C_6H_6 (g). With the knowledge of the C_6H_6 surface concentration, the three variables that remain
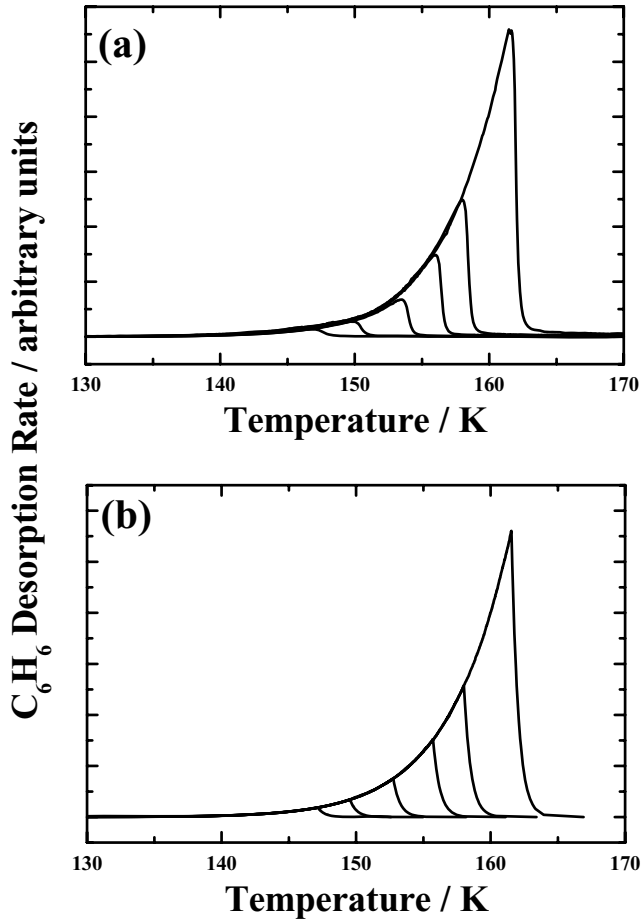

Figure 5. (a) TPD traces for C$_6$H$_6$ multilayer desorption. Exposures are 10, 20, 50, 100, 200 and 500 L. (b) Shows the simulated TPD traces that result from a zero-order kinetic model with $E_{des}/k_B = 5600$ K and $\nu = 5 \times 10^{29}$ molecules cm^{-2} s^{-1}.

unknown are the pre-exponential factor for the desorption step, the desorption energy and the pre-exponential factor for the pumping step, hereafter referred to as the pumping speed. Using this model, TPD spectra were simulated for the case of multilayer desorption for raw exposures of 10, 20, 50, 100, 200 and 500 L. Zero-order desorption kinetics (i.e. $n = 0$) were assumed given the good coincidence of the leading edges. ν, E_{des} and the pumping speed were systematically varied and resulting simulated traces were compared with the experimental results through the use of an appropriate scaling factor. Fig. 5 shows a comparison between the experimental and simulated TPD traces for large exposures of C$_6$H$_6$. The experimental data are best simulated with a ν value of $10^{29.7\pm1.0}$ molecules cm^{-2} s^{-1} and an E_{des}/k_B value of 5600 ± 100 K (46.6 ± 0.8 kJ mol^{-1}). It is clear that these kinetic parameters describe the experimental TPD traces well over a large exposure range. There is some small deviation from the experimental data for the lowest exposure simulations, which likely results from the desorption order becoming slightly non-zero. This is consistent with the clearly fractional-order desorption kinetics observed at exposures of around 10 L, evidenced by non-coincident leading edges. With our approach, it is not possible to obtain reliable results from simulations of fractional-order desorption due to the introduction of another unknown variable. The value for E_{des} is in good agreement with reported values for the sublimation en-

ergy of condensed C$_6$H$_6$, which generally lie in the range of 44–47 kJ mol^{-1} (Chickos & Acree 2002) and with previously reported values for the desorption of multilayers of C$_6$H$_6$ from metal surfaces (see, e.g., Jakob & Menzel 1989).

It is clear that the desorption of C$_6$H$_6$ is complicated by the presence of pores, which has a large impact on the desorption profile. A combination of further experimental work and more detailed analysis will be required to fully understand the effect that this porosity has on the desorption process. This is discussed in more detail in the Conclusions section of this paper. However, it is possible to obtain a general insight by modelling the desorption using first-order desorption kinetics. In this approximation, the steps involved in escaping from the pores are combined into one simple desorption step. Whilst this clearly oversimplifies the desorption process, it is useful in providing an indication of kinetic parameters. Two approaches were used to observe the trends in the desorption energy, E_{des}, and the pre-exponential factor, ν, as a function of C$_6$H$_6$ exposure. In the first instance, the TPD traces were analysed by assuming a pre-exponential factor of 10^{13} s^{-1}, as in the frequently invoked Redhead method (Attard & Barnes 1998). Rather than using the Redhead expression directly, the TPD traces were simulated using the kinetic modelling procedure described above to obtain the desorption energy. Our approach was to fit the leading edge of the desorption trace, corresponding to simple first-order desorption. The presence of the tail due to desorption from pores makes the determination of the surface concentration minus the tail component difficult. However, by using the pumping speed and the scaling factor obtained during the multilayer analysis, the only unknown variables were E_{des} and the surface concentration. These were then systematically varied to obtain the best values. This analysis reveals a wide range of values for E_{des}/k_B, decreasing from 6250 K (52 kJ mol^{-1}) at the lowest exposure to 4800 K (39.5 kJ mol^{-1}) at exposures of around 1 L. The obtained E_{des}/k_B values are shown in Table 1. As discussed previously, we expect the actual range of binding energies to be somewhat smaller than this. Some distribution of binding energies is likely to arise due to increased coordination within the pore network.

Given the complicated nature of the surface, it is highly probable that the assumption that ν does not vary with coverage will not hold. For this reason, an independent method was used to obtain values for E_{des}. This method has been described previously (Bolina et al. 2005), and is derived by considering that the QMS signal, $I(T)$, is directly proportional to the desorption rate:

$$I(T) \propto N^n \nu \exp(-E_{des}/k_B T), \qquad (7)$$

which can be rearranged to yield

$$\ln[I(T)] \propto n \ln[\nu] + n \ln[N] - E_{des}/k_B T. \qquad (8)$$

Thus for a given TPD experiment, a plot of $\ln[I(T)] - n \ln[N]$ versus $1/T$ for the leading edge will have a gradient of $-E_{des}/k_B$, from which the desorption energy can be obtained. The value for E_{des}/k_B resulting from this analysis is 5300 ± 200 K (44 ± 2 kJ mol^{-1}). In this analysis, this value is independent of coverage in the sub-monolayer regime. The uncertainty on this value is larger than for that obtained for multilayer desorption because of the significantly lower signal-to-noise ratio in the low-coverage regime. This value was then used to obtain corresponding ν values using appropriate kinetic modelling to reproduce the leading edge of the desorption traces. The values of ν that were obtained ranged from 4×10^{10} s^{-1} at the lowest exposure to 7×10^{14} s^{-1} at exposures of around 1 L. The obtained ν values are shown in Table 1. Fig. 6 shows a comparison between (a) the experimental TPD traces and

Table 1. Kinetic parameters obtained for the desorption of C_6H_6 from the SiO_2 surface. The surface concentrations are those that best reproduce the experimental data based on the pumping speed and scaling factor obtained from the multilayer analysis. Both E_{des} values for a fixed value of $\nu = 10^{13}$ s^{-1} (the Redhead model) and ν values obtained for a fixed E_{des}/k_B value of 5300 K (obtained from the leading edge analysis) are shown.

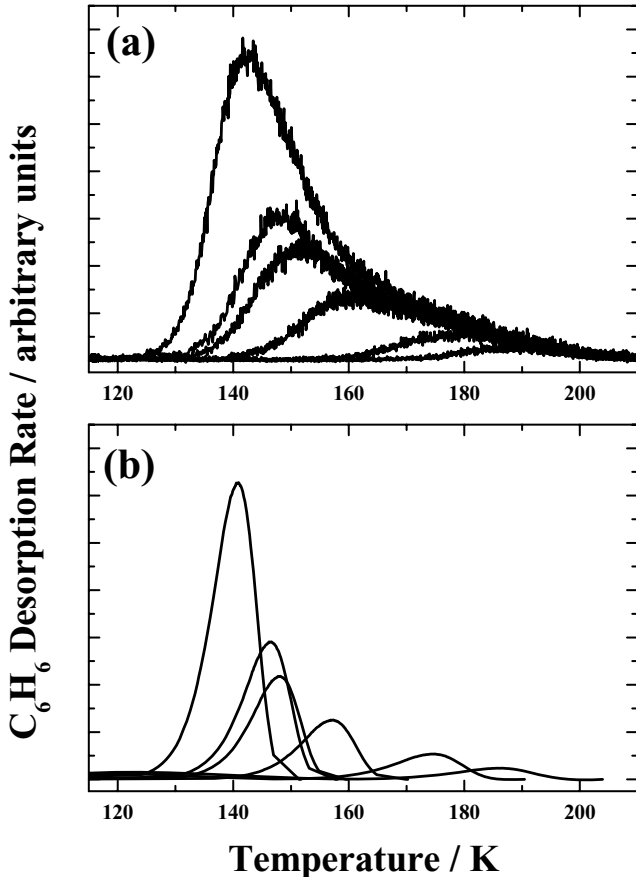| C_6H_6 exposure/L	C_6H_6 surface concentration/molecules cm^{-2} (excluding pore contribution)	$E_{des} k_B^{-1}$/K ($\nu = 1 \times 10^{13}$ s^{-1})	ν/s^{-1} ($E_{des}/k_B = 5300$ K)
0.1	$(1.0 \pm 0.5) \times 10^{12}$	6250	4.0×10^{10}
0.2	$(2.0 \pm 0.5) \times 10^{12}$	5890	3.0×10^{11}
0.5	$(4.0 \pm 0.5) \times 10^{12}$	5290	1.1×10^{13}
0.7	$(7.0 \pm 0.5) \times 10^{12}$	4990	1.0×10^{14}
0.8	$(9.5 \pm 0.5) \times 10^{12}$	4930	1.5×10^{14}
1	$(1.9 \pm 0.5) \times 10^{13}$	4750	7.0×10^{14}

Figure 6. (a) TPD traces for the desorption of C_6H_6 from amorphous SiO_2. Exposures are 0.1, 0.2, 0.5, 0.7, 0.8 and 1 L. (b) Shows the simulated TPD traces first-order kinetic modelling. The fixed value of $E_{des}/k_B = 5300$ K was obtained from leading edge analysis of the experimental traces.

(b) those obtained from kinetic modelling. The small values of ν at low coverages are unphysical, and demonstrate the limitations of modelling pore escape as a one-step process. At larger coverages, ν increases to values that would be expected for simple first-order desorption. The large increase in ν in going from 0.8 to 1 L is likely related to the restructuring of the monolayer observed as Peak B in Fig. 2. Such restructuring, which occurs as a result of repulsive interactions between C_6H_6 molecules as the monolayer becomes more crowded, has been observed previously in studies of C_6H_6 adsorption on single crystal surfaces. Waddill & Kesmodel (1985) observed the appearance of a TPD peak at lower temperature as the

C_6H_6 coverage on both Pd(111) and Pd(100) was increased towards monolayer saturation and attributed this to repulsive interactions. Repulsive interactions can have a significant effect on the observed desorption energy of a molecule, in the case of C_6H_6 on Pd(111). Monte Carlo simulations (Tysoe et al. 1993) have shown the repulsion energy to be 6.5 kJ mol^{-1} (780 K). Whilst in these experiments the C_6H_6 was chemisorbed on the substrate resulting in significantly higher desorption energies than observed in our experiment, where the C_6H_6 is more weakly bound, there is no reason to assume that the repulsive interaction would be significantly different. In some cases, for example on polycrystalline Ag (Bahr & Kempter 2007), the increase in intermolecular repulsion has been shown to result in the formation of a second layer where the C_6H_6 molecules are adsorbed with their plane tilted with respect to the substrate. This reduces the overlap between the C_6H_6 π orbitals and substrate orbitals, resulting in a decrease in desorption energy.

On SiO_2, C_6H_6 is likely to form weak hydrogen bonds with OH groups on the hydroxylated surface as has been observed in gas-phase C_6H_6–H_2O clusters (Suzuki et al. 1992). However, we have no specific evidence from these experiments to support this. The roughness of the surface means that C_6H_6 will not be bound in one particular orientation, rather it will adopt a distribution of orientations that optimizes the binding energy. As the coverage is increased, repulsive interactions increase, resulting in some restructuring of the monolayer. This leads to a decreased desorption energy and an increasing pre-exponential factor.

4 ASTROPHYSICAL IMPLICATIONS

The experiments outlined here demonstrate the complexity of the interaction between molecules and dust grain surfaces. Surface roughness and the presence of pores have a large impact on the desorption of C_6H_6 from such surfaces, particularly at low coverages. The desorption kinetics are affected by interactions between adjacent C_6H_6 molecules, the heterogeneous nature of the SiO_2 surface and the presence of pores within the film. These results indicate that the nature of C_6H_6 adsorption is likely to be sensitive to the astrophysical environment in which the grain is situated.

We first consider grains in the dense ISM where C_6H_6 abundance is expected to be relatively low due to destruction by interaction with UV photons. The distribution of adsorbed C_6H_6 will depend on the C_6H_6 mobility, and therefore the grain temperature. As grains in the ISM tend to be at the lowest temperatures, C_6H_6 mobility will be reduced making it unlikely that C_6H_6 molecules will penetrate as far into the pore network as they would at high temperatures when mobility is much higher. The TPD experiments described here probe the high-mobility regime as molecules will become mobile

during warm-up. This same migration due to increased mobility will also occur as grains warm, though the extent to which molecules penetrate the pore network will depend on the presence of any other species that may block access to the pores. The relative mobilities of these species will also be important as observed through the experiments where the surface was first exposed to H_2O. Such a situation would occur in the dense ISM where significant amounts of H_2O ice tend to be adsorbed on to grain surfaces. Under these circumstances, mobile C_6H_6 is unable to penetrate the pore network if the H_2O has previously been sufficiently mobile to penetrate, or there is sufficient H_2O to block access to the pores. The resulting desorption would then be dominated by the kinetics observed at exposures of around 1 L in these experiments, where intermolecular repulsion plays an important role.

This behaviour will also have important consequences for the return of C_6H_6 to the gas phase following formation in protostellar discs. The efficiency of this process will depend on the residence time of C_6H_6 on the grain surface which will in turn depend on the grain temperature and the C_6H_6–grain interaction. However, whilst we expect the binding energy between C_6H_6 and a silicate grain surface to be fairly uniform across the surface, this will be modified by the presence of any pre-adsorbed species. If the grain temperature is sufficiently low to allow formation of a monolayer of C_6H_6, or significant H_2O ice is present then intermolecular repulsion will lead to a more efficient return of C_6H_6 to the gas phase than would be expected from a simple consideration of grain temperature and binding energy alone. It is also important to note that carbonaceous grains are likely to dominate in such an environment. The interaction between C_6H_6 and, for example, a graphitic surface will be significantly different, though the arguments presented here relating to intermolecular repulsion and the presence of adsorbed H_2O would be expected to hold.

Whilst absorption in pores has a strong effect on the experimental desorption profiles obtained with a heating rate of 0.1 K s^{-1}, it is likely that this is not the case at astronomical heating rates. We are currently developing a simple kinetic model to describe the desorption from pores in terms of the mechanism described previously. This model will be based on our previous model for the desorption of CO from porous H_2O films (Collings et al. 2003). Initial results suggest that as the heating rate is lowered the desorption profile tends towards simple first-order kinetics. This can be interpreted as the desorption from the surface becoming the rate limiting step, rather than the escape from pores. It may therefore be most appropriate to consider the kinetic parameters obtained for the high-coverage regime ($\sim$1 L) to be most suitable in astrophysical environments.

While the abundance of C_6H_6 in astrophysical environments is unlikely to be sufficient for the formation of thick ice layers on grain surfaces, the importance of the multilayer measurements reported here should be highlighted. The kinetic parameters derived are related to the interactions between C_6H_6 molecules, rather than between C_6H_6 molecules and the underlying substrate. Such interactions become important in the first few layers beyond the monolayer. Furthermore, as discussed, C_6H_6 tends to form islands on a H_2O ice surface, with the interactions within these islands more closely resembling those in the multilayer regime.

5 CONCLUSIONS

We have reported the results of a series of TPD experiments investigating the adsorption of C_6H_6 on a dust grain mimic based on amorphous SiO_2. The desorption kinetics of both substrate-bound and multilayer C_6H_6 have been studied in detail through a combination of direct analysis and kinetic modelling using stochastic integration of the differential equations describing the desorption process. The desorption of C_6H_6 multilayers from adsorbed bulk C_6H_6 ice displays simple zero-order kinetics with a desorption energy of 5600 ± 100 K and a pre-exponential factor of $10^{29.7\pm1.0}$ molecules cm^{-2} s^{-1}, in good agreement with previous studies. However, the desorption of small amounts of C_6H_6 from the SiO_2 surface demonstrates the effect the underlying surface can have on the desorption process. The presence of pores within the SiO_2 and a rough surface, along with the effect of repulsive interactions between C_6H_6 molecules, leads to complicated desorption kinetics within the first few C_6H_6 layers. At low coverages, the desorption of C_6H_6 molecules from within pores has an important influence on the desorption profile. C_6H_6 molecules bound within pores are likely to be re-adsorbed several times before desorbing from the surface. This leads to a high-temperature tail being superimposed on the peak related to desorption from the SiO_2 surface. Increasing C_6H_6 coverage towards monolayer saturation leads to an increased repulsion between C_6H_6 molecules, resulting in a decreased surface binding energy and an increased pre-exponential factor. It is clear that in order to gain a better understanding of the adsorption on grain surfaces, the coverage dependencies of the kinetic parameters need to be isolated. In particular, our kinetic model needs to be modified to specifically include a description of the desorption from pores. Such a model would include both re-adsorption and gas-phase diffusion steps in order to isolate the kinetic parameters for the desorption process. Further insights into the desorption process will be aided by experiments performed on a flat, crystalline SiO_2 surface with no pores, which will help to identify the morphological effects of the grain surface on desorption kinetics. This work has demonstrated the sensitivity of the desorption process to both physical and chemical conditions in the local environment.

REFERENCES

Allamandola L. J., Hudgins D. M., Sandford S. A., 1999, ApJ, 511, L115
Arnett E. M., Hutchinson B. J., Healy M. H., 1988, J. Am. Chem. Soc., 110, 5255
Atkins P., de Paula J., 2002, Physical Chemistry, 7th edn. Oxford Univ. Press, Oxford
Attard G., Barnes C., 1998, Surfaces. Oxford Univ. Press, Oxford
Bahr S., Kempter V., 2007, J. Chem. Phys., 127, 074707
Bernstein M. P., Sandford S. A., Allamandola L. J., 2005, ApJS, 161, 53
Bernstein M. P., Sandford S. A., Mattioda A. L., Allamandola L. J., 2007, ApJ, 664, 1264
Bolina A. S., Wolff A. J., Brown W. A., 2005, J. Phys. Chem. B, 109, 16836
Bregman J. D., Temi P., 2001, ApJ, 544, 126
Cernicharo J., Heras A. M., Tielens A. G. G. M., Pardo J. R., Herpin F., Guelin M., Waters L. B. F. M., 2001, ApJ, 546, L123

Cherchneff I., Berker J. R., Tielens A. G. G. M., 1992, ApJ, 401, 269

Chickos J. S., Acree W. E., 2002, J. Phys. Chem. Ref. Data, 31, 537

Collings M. P., Dever J. W., Fraser H. J., McCoustra M. R. S., 2003, Ap&SS, 285, 633

Duley W. W., 2006, Faraday Discuss., 133, 415

Ehrenfreund P., Sephton M. A., 2006, Faraday Discuss., 133, 277

Flagey N., Boulanger F., Verstraete L., Miville Deschênes M. A., Noriega Crespo A., Reach W. T., 2006, A&A, 453, 969

Fraser H. J., Collings M. P., McCoustra M. R. S., Williams D. A., 2001, MNRAS, 327, 1165

Frenklach M., Feigelson E. D., 1989, ApJ, 341, 372

Garrod R. T., Herbst E., 2006, A&A, 457, 927

Haq S., King D. A., 1996, J. Phys. Chem., 1996, 100, 16957

Hasegawa T. I., Herbst E., 1993, MNRAS, 261, 83

Houle F. A., Hinsberg W. D., 1995, Surf. Sci., 338, 329

Jakob P., Menzel D., 1989, Surf. Sci., 220, 70

Kaneda H., Onaka T., Sakon I., 2005, ApJ, 632, L83

Kassis M., Adams J. D., Campbell M. F., Deutsch L. K., Hora J. L., Jackson J. M., Tollestrup E. V., 2006, ApJ, 637, 823

Lagadec E. et al., 2006, A&A, 448, 203

Lozovik Y. E., Popov A. M., Letokhov V. S., 1995, J. Phys. Chem., 99, 13480

McEwan M. J., Scott G. B. I., Adams N. G., Babcock L. M., Terzieva R., Herbst E., 1999, ApJ, 513, 287

Mautner M. N., Abdelsayed V., El-Shall M. S., Thrower J. D., Green S. D., Collings M. P., McCoustra M. R. S., 2006, Faraday Discuss., 133, 103

Oakes D. J., 1994, PhD thesis, Univ. East Anglia

Ristorcelli I., Klotz A., 1997, A&A, 317, 962

Rockey T. J., Yang M., Dai H.-L., 2006, J. Phys. Chem. B., 110, 19973

Ruiterkamp R., Peeters Z., Moore M. H., Hudson R. L., Ehrenfreund P., 2005, A&A, 440, 391

Sandford S. A., Bernstein M. P., Allamandola L. J., 2004, ApJ, 607, 346

Smith J. D. T. et al., 2007, ApJ, 656, 770

Suzuki S., Green P. G., Bumgarner R. E., Dasgupta S., Goddard W. A., Blake G. A., 1992, Sci, 257, 942

Thrower J. D. et al., 2008, ApJ, 673, 1233

Tielens F., Gervais C., Lambert J. F., Mauri F., Costa D., 2008, Chem. Mater., 20, 3336

Tysoe W. T., Ormerod R. M., Lambert R. M., Zgrablich G., Ramirez-Cuesta A., 1993, J. Phys Chem, 97, 3365

Waddill G. D., Kesmodel L. L., 1985, Phys. Rev. B, 31, 4940

Woods P. M., Willacy K., 2007, ApJ, 655, L49

Woods P. M., Miller T. J., Zijlstra A. A., 2002, Herbst E., ApJ, 574, L167

This paper has been typeset from a Microsoft Word file perpared by the author.